Macromolecules

pubs.acs.org/Macromolecules Article

Lyotropic Phase Behavior of Coil-Bottlebrush Diblock Copolymers in Alkylimidazolium-Based Ionic Liquids

Camila Perales Rodriguez, Mahesh K. Mahanthappa,* and Timothy P. Lodge*

Cite This: *Macromolecules* 2024, 57, 3081−3089 Read Online

ACCESS | Metrics & More | Article Recommendations | Supporting Information

ABSTRACT: Block copolymer melts self-assemble into 3D network (NET) nanostructures, exhibiting useful, nonlinear combinations of the properties of their constituents. However, chain packing frustration limits NET formation to specific and narrow composition windows in linear diblocks. While recent work has demonstrated that the location of the NET window in coil-*block*-bottlebrush diblocks may be tuned by varying the brush architecture, the composition window remains narrow. Aiming to widen access to NETs, we explore the lyotropic self-assembly of coil-*block*-bottlebrush diblocks in the presence of coil-selective *N*-alkyl-*N*′-methylimidazolium bis(trifluoromethylsulfonyl)imide ionic liquids [C_xMIM][TFSI], where C_x is an *n*-alkyl substituent with x = 1, 4, 6, 8, 10, or 12 carbons. Morphological analyses of these IL lyotropic assemblies based on diblocks with coil volume fractions $f_{coil} \approx 0.38$ indicate the formation of various coexisting morphologies. Despite significant variations in solvent selectivity with x, the lyotropic phase behavior exhibits a surprisingly weak dependence on IL identity.

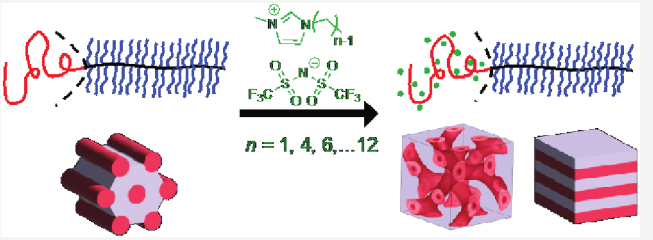

INTRODUCTION

Block copolymer (BCP) self-assembly offers an attractive approach for designing multifunctional materials with tailored morphologies, properties, and functionalities that arise from the underlying polymer segment chemistries.[1,2] Their microphase separation enables access to spatially periodic nanostructures that find applications as isoporous separation membranes,[3] nanotemplates for inorganic materials,[4−6] and solid polymer electrolytes for batteries.[7,8] The propensity for AB diblock copolymers to undergo self-assembly depends on the segregation strength χN, where N is the total volume-referenced degree of polymerization, and χ is the effective interaction parameter quantifying the energetic repulsion between dissimilar monomer segments.[9] Above a critical value of χN, these macromolecules form ordered spherical micelle packings (SPH), hexagonally packed cylinders (HEX), lamellae (LAM), and 3D network morphologies (NETs) exemplified by the double gyroid (GYR).[10,11] Phase selection primarily depends on the copolymer volume composition, $f_A = 1 - f_B$, with a modest dependence on the value of χN.

NETs are particularly attractive BCP morphologies because of their percolating and interpenetrating three-dimensional microdomain structures,[12−14] which enable orthogonal tunability of the thermomechanical and transport properties in selective ion[15] and water[16] transporting membranes, internally structured therapeutic nanoparticles,[17] and nanostructured materials for energy conversion devices.[18−20] To date, experimentally observed NETs in diblock copolymers include GYR,[21,22] double diamond (DD),[23−25] and the O^{70} network,[26,27] with $Ia\bar{3}d$, $Pm\bar{3}m$, and $Fddd$ space group symmetries, respectively. However, the packing frustration associated with the nonconstant mean curvature domain interfaces in NETs restricts their stability to narrow and specific polymer composition windows in prototypical linear diblocks.[28,29] This ultimately constrains their widespread applications.

One possible means of broadening access to NET phases relies on the incorporation of block-selective solvents to produce lyotropic mesophases with solvent concentration-dependent morphologies.[30−33] Preferential localization of a block-selective solvent in one microdomain changes the effective volume fraction (φ_{eff}) and effective χ_{eff} of the BCP.[34] Consequently, varying the amount of solvent allows one to traverse the block copolymer morphology diagram using a single copolymer sample,[30,32] with the added possibility of accessing new morphologies not found in the neat diblock copolymer melt.[35] For example, Kim and coworkers have demonstrated conditions for the aqueous self-assembly of amphiphilic diblock copolymers into internally structured colloidal particles exhibiting DG, DD, and even double-primitive NET morphologies.[36] While BCP self-assembly in

Received: November 27, 2023
Revised: March 7, 2024
Accepted: March 11, 2024
Published: March 28, 2024

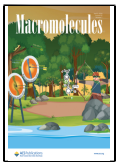

https://doi.org/10.1021/acs.macromol.3c02451
Macromolecules 2024, 57, 3081−3089

Scheme 1. Living ROMP Synthesis of MP_4 Coil-Brush Diblock Copolymers

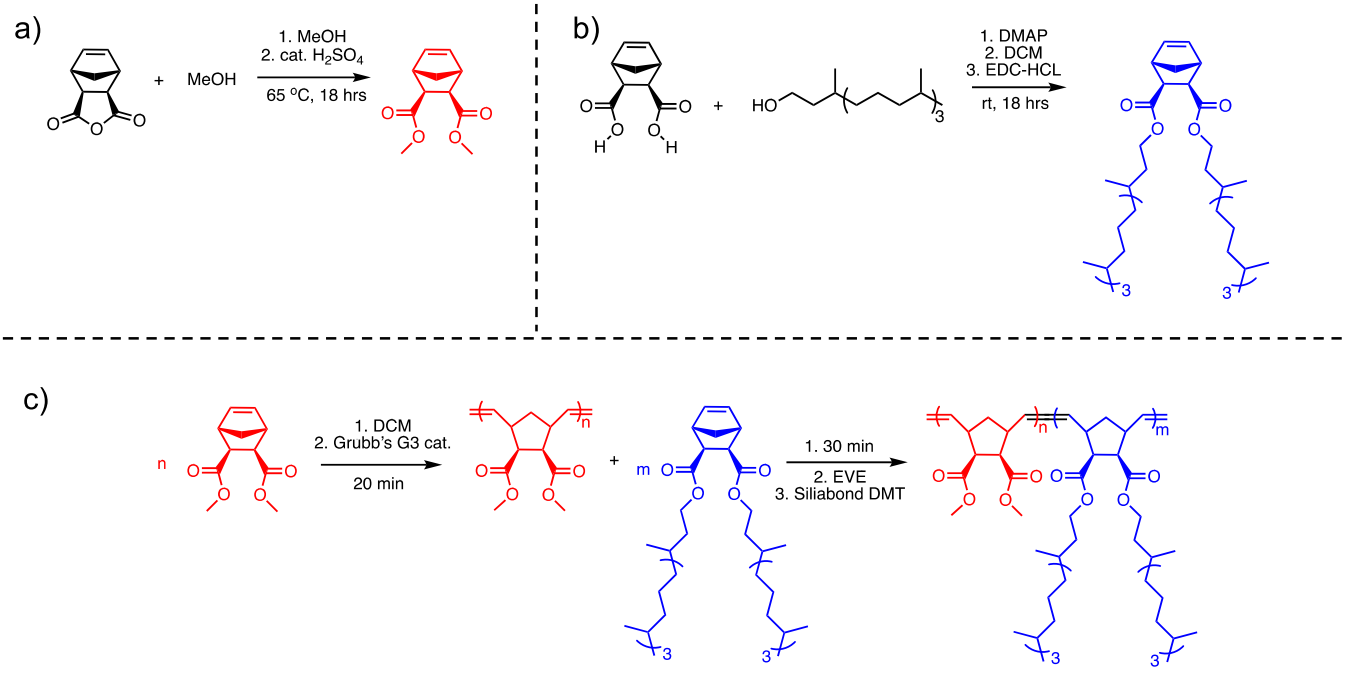

aqueous and organic solvents is well-documented,[30,31,34,37−40] studies of their lyotropic assembly in ionic liquids (ILs)[41] have primarily focused on dilute micellar solutions[42−44] with more limited attention to self-assembly phase behavior in the concentrated limit.[43,45−49] Ionic liquids are of interest due to their negligible vapor pressures, high thermal stabilities, and low viscosities,[50] which confer application-specific added value to copolymer assemblies.[51−54] For example, Bennett et al.[46] demonstrated that adding a small amount of an IL to disordered poly(styrene)-*block*-poly(methyl methacrylate) (PS-*b*-PMMA) diblock copolymers drives their microphase separation, by IL segregation into the PMMA domains with an attendant increase in χ_{eff}. Chen et al. subsequently translated these results into BCP thin films to achieve sub-10 nm patterning using IL-doped PS-*b*-PMMA.[47]

While the lyotropic self-assembly behavior of linear diblock copolymers is relatively well-explored, comparatively less is known about lyotropic phase selection in more complex diblock architectures. Liberman et al. recently reported the synthesis and self-assembly behavior of architecturally asymmetric coil-bottlebrush diblock copolymers as a means of expanding the width of NET composition window and tuning its location.[55,56] By increasing the bottlebrush side chain length, they demonstrated that increasing architectural asymmetry shifts the DG morphology window to higher f_{coil} values with modest increases in the composition-dependent stability window.[55] Building on that work, we herein investigate the possibility of widening access to NETs of coil-bottlebrush diblock copolymers by the inclusion of IL solvents. We specifically focus on the lyotropic phase behaviors of two HEX-forming coil-bottlebrush block copolymers with $f_{coil} \approx 0.4$, which derive from living ring-opening metathesis polymerization (ROMP) of dialkyl esters of 5-norbornene-2,3-*exo*,*exo*-dicarboxylic acid, in the presence of six coil-selective alkylimidazolium-based ILs. We evaluate the viability of using this lyotropic approach to tune the volume fractions over which bicontinuous NETs assemble with the concomitant possibility of accessing larger domain periodicities by selective microdomain swelling.

EXPERIMENTAL SECTION

Materials. *cis*-5-Norbornene-2,3-*exo*,*exo*-dicarboxylic anhydride was obtained from TCI America (Portland, OR, USA). Phytol was purchased from ApexBio (Houston, TX, USA), and SiliaBond DMT was obtained from Thermo Fisher Scientific (Pittburgh, PA, USA). Ionic liquids were purchased from IoLiTec (Heilbronn, Germany) and purified as reported in the Supporting Information. All other reagents were purchased from Millipore-Sigma (Milwaukee, WI, USA) and used without further purification. CH_2Cl_2 was degassed by sparging with high-purity argon and dried by passage through activated alumina in a Vacuum Atmospheres Inc. solvent purification system and used inside an argon-filled glovebox. $CDCl_3$, $(CD_3)_2SO$, and C_6D_6 for ^1H NMR spectroscopy were purchased from Cambridge Isotopes Laboratories (Andover, MA, USA). TZero and standard hermetic aluminum sample pans for small-angle X-ray scattering (SAXS) were obtained from DSC Consumables, Inc. (Austin, MN, USA).

Size-Exclusion Chromatography with Multiangle Light Scattering (SEC-MALS). Polymer samples comprising ∼5 mg of polymer in 1 mL of THF (ACS reagent, ≥ 99.9% inhibited with 250 ppm of BHT) were filtered through 0.22 μm polytetrafluoroethylene (PTFE) syringe filters prior to analysis. Samples were then analyzed using an Agilent Technologies SEC instrument equipped with a Tosoh Styragel guard column and three TSKgel G6000-Hhr columns (7.8 mm × 30 cm) packed with 5 μm diameter poly(styrene-*co*-divinylbenzene) particles. The weight-average molecular weight (M_w), number-average molecular weight (M_n), and dispersity ($Đ = M_w/M_n$) were determined by using a Wyatt Technology DAWN Heleos II 18-angle light-scattering detector operating at a wavelength of 658 nm and a Wyatt Optilab T-rEX refractive index detector. The $\partial n/\partial c$ for each copolymer was calculated as a weighted average of the measured refractive index increments of the constituent homopolymers: 5-norbornene-2,3-*exo*,*exo*-dicarboxylate acid dimethyl ester to yield a coil segment denoted **M** and 5-norbornene-2,3-*exo*,*exo*-dicarboxylic acid bis(phytol) ester as the bottlebrush block denoted $\mathbf{P_4}$ (Scheme 1). The $\partial n/\partial c$ values for $MP_4(5-10)$ and $MP_4(7-13)$ were calculated to be 0.0856 and 0.0817 mL/g, respectively.

https://doi.org/10.1021/acs.macromol.3c02451
Macromolecules 2024, 57, 3081−3089

Small-Angle X-Ray Scattering (SAXS). Synchrotron SAXS measurements were performed at the 12-ID-B and 5-ID-D beamlines at the Advanced Photon Source (Argonne, IL. USA). THF solutions containing measured amounts of polymer and ionic liquid were solvent cast into TZero DSC pans at 60 °C. The samples were then annealed under a vacuum at 140 °C for 2 h to remove residual THF, prior to hermetically sealing them under argon. The samples were subsequently annealed in a vacuum oven at 140 °C for 24 h and slowly cooled to ambient temperature. Unless otherwise noted, samples remained at ambient temperature for 1 week prior to SAXS analysis. Synchrotron SAXS data were acquired at the 12-ID-B beamline of the Advanced Photon Source (APS) at Argonne National Laboratory using an X-ray wavelength λ = 0.886 Å with a 3.6 m sample-to-detector distance using an EIGER2 S 1 M detector with a 77.1 mm × 79.7 mm active area. Alternatively, additional synchrotron SAXS data were collected at the 5-ID-D beamline of the APS, using λ = 0.729 Å X-rays and an 8.5 m sample-to-detector distance on an annular MAR-CCD detector (active area 100 mm × 100 mm). In both cases, samples were heated or cooled to a target temperature 25 ≤ T ≤ 180 °C and equilibrated for 15 min using a custom-built multiarray heating stage available at the beamline, prior to X-ray exposure for 0.1 s to obtain two-dimensional (2D) SAXS patterns. Isotropic 2D-SAXS patterns were azimuthally averaged to obtain one-dimensional (1D) scattering intensity profiles as a function of q using software macros available at each beamline end station. These SAXS profiles were analyzed using a freely available SAXS analysis macro[57] implemented in the IGOR Pro (WaveMetrics, Inc.) software environment.

RESULTS AND DISCUSSION

To study the effect of selective IL solvent addition to an architecturally asymmetric BCP, we chose a previously characterized coil-*block*-bottlebrush system.[55] Liberman et al. used a modular norbornyl monomer synthesis in conjunction with sequential living ring-opening metathesis polymerization (ROMP) to produce extensive polycyclopentenamer libraries of coil-bottlebrush diblock copolymers with varied coil and brush segment chemistries for comparative phase behavior studies. Herein, we focused on two **MP$_4$** diblocks with different backbone degrees of polymerization (N_{bb}) derived from sequential living ROMP (Scheme 1). Representative ^{1}H NMR spectra and SEC analyses given in Figures S1−S6 demonstrate the successful syntheses of two diblocks with well-defined molecular compositions and low molar mass dispersities ($Đ = M_w/M_n$), per the prior report. We targeted the syntheses of diblocks with compositions $f_M \approx 0.38$ in the proximity of the expected NET phase window. Detailed molecular characterization information for these polymers is given in Table 1.

Table 1. Molecular Characteristics of Coil-Brush Diblock Copolymers Used

sample[a]	M_n (kg/mol)[b]	$Đ$[b]	f_M[c]	N_{bb}[d]	N[e]
MP$_4$(5−10)	15.5	1.03	0.37	44	210
MP$_4$(7−13)	19.4	1.03	0.39	56	262

[a]Numbers in parenthesis represent the M_n (kg/mol) of each block, with the first number corresponding to the coil **M** block. [b]Determined by SEC-MALS at 22 °C. [c]f_M is the **M** block volume fraction determined by ^{1}H NMR spectroscopy. [d]N_{bb} is the total backbone degree of polymerization calculated using SEC-MALS and ^{1}H NMR spectroscopy. [e]Segment density-normalized degree of polymerization (N) calculated against a 118 Å^3 reference volume at 22 °C, using ρ_{coil} and ρ_{brush} as 1.240 and 0.915 g/cm^3, respectively, as in ref. 55.

IL-containing diblock copolymer assemblies were produced by codissolution of measured amounts of a given copolymer and ionic liquid in THF as a common solvent. These solutions were then solvent cast at 60 °C, followed by THF removal under a vacuum at 140 °C and subsequent thermal annealing at 140 °C for 24 h. The process was applied to MP$_4$(5−10) and MP$_4$(7−13) with each of the six ionic liquids C$_1$−C$_{12}$, where C$_x$ refers to the *N*-*n*-C$_x$H$_{2x+1}$-*N*′-methyl-imidazolium bis(trifluoromethylsulfonyl)imide ([*n*-C$_x$H$_{2x+1}$MIM][TFSI]) with x = 1, 4, 6, 8, 10, 12 to produce >60 distinct samples. These samples collectively enabled mapping of six different lyotropic self-assembly phase diagrams targeted around the IL contents expected to produce NET phases. Note that all of these ILs are expected to be coil block-selective to varying degrees based on relative polarity considerations. The polymer volume fractions in these two-component assemblies were calculated as

$$\varphi = \frac{m_{MP_4}/\rho_{MP_4}}{m_{MP_4}/\rho_{MP_4} + m_{IL}/\rho_{IL}} \quad (1)$$

and spanned the range 0.7 ≤ φ ≤ 0.98, where m_i and ρ_i are the respective masses and densities of species i in each binary mixture. The mass densities of the C$_x$ ionic liquids are given in Table S1.

Synchrotron small-angle X-ray scattering (SAXS) was used to assess sample morphologies at 140 °C as functions of both N and φ for MP$_4$(5−10) and MP$_4$(7−13) approximately 1 week after sample preparation (see Experimental Section for data acquisition details). Representative SAXS patterns for MP$_4$(7−13) with different concentrations of C$_6$ obtained at 140 °C are shown in Figure 1a. The broad SAXS peaks for MP$_4$(7−13) located at $(q/q^*)^2$ = 1, 3, 4, 7, 11, and 12 with q^* = 0.0294 Å^{-1} correspond to a HEX morphology with domain spacing $d = 2\pi/q^*$ = 21.3 nm. Based on the coil block volume fraction f_M = 0.39, this microphase-separated structure consists of M-rich cylinders in a P$_4$ matrix. Upon addition of the C$_6$ IL such that φ = 0.83, we obtained an SAXS pattern consistent with a LAM phase with five characteristic SAXS peaks at q/q^* = 1, 2, 3, 4, and 5 with lamellar periodicity d = 23.4 nm. Note that the LAM d-spacing changes very little as the IL content increases to φ = 0.71, albeit with changes in the relative peak intensities indicative of changes in the solvent volume fraction. The intervening sample compositions between the pure LAM and HEX morphologies generate more complex scattering patterns consistent with two-phase coexistence. When φ = 0.95−0.91, we obtained SAXS patterns indicative of coexisting HEX and GYR morphologies. The GYR morphology generally exhibits SAXS peaks at $(q/q^*)^2$ = 6, 8, 14, 16,⋯ with lattice constants d = 51.2−53.2 nm at these IL contents. Note that increasing the IL content (decreasing φ) drives increases in the d-spacings of both the HEX and GYR morphologies, until the critical value φ = 0.85 when the sample transitions to HEX coexisting with LAM. Additional SAXS patterns can be found in the Figures S7−S9.

Variable-temperature SAXS studies revealed that heating these C$_6$ samples to higher temperatures did not necessarily trigger the resolution of phase coexistence into a dominant morphology. For example, a sample comprising MP$_4$(7−13) with φ = 0.91 transitions from clear HEX/GYR coexistence into what appears to be predominantly a GYR phase upon heating (Figure 1b), based on the higher intensities of the cubic SAXS peaks. However, careful indexing of this SAXS

https://doi.org/10.1021/acs.macromol.3c02451
Macromolecules 2024, 57, 3081−3089

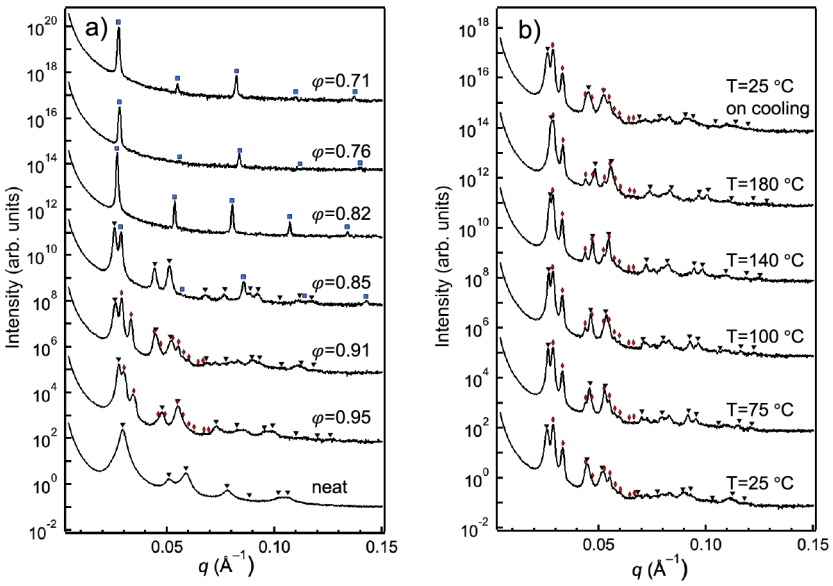

Figure 1. Representative SAXS patterns for $MP_4(7-13)$ (a) in the IL C_6 at 25 °C and (b) a temperature sweep for a sample formed at $\varphi = 0.91$ peak markers indicate the various observed phases: LAM (*blue squares*), HEX (*black triangles*), and GYR (*red diamonds*). Additional patterns can be found in the Supporting Information.

pattern reveals a substantial number of higher-order SAXS peaks consistent with a HEX morphology, with a q^* peak that is nearly coincident with the $q^*\sqrt{6}$ peak ((211) reflection) of the GYR phase. These observed temperature-dependent order-to-order transitions (OOTs) are mostly reversible on cooling. Heating samples exhibiting ambient temperature phase coexistence with more intense SAXS peaks for one morphology generally drive them toward that dominant morphology, as shown in Figure S7. In cases where the ambient temperature SAXS peak intensities for each morphology are comparable, the dominant morphology at higher temperatures becomes harder to anticipate, as illustrated in Figure S8.

Impact of Solvent Selectivity on Self-Assembly Behavior. The results of the above SAXS analyses for lyotropic samples of the two MP_4 samples in the six IL solvents C_1-C_{12} are compiled in Figure 2 as binary phase diagrams plotted as N/T versus φ, where N is the segment density-normalized degree of polymerization relative to a reference volume calculated as

$$N = \left(\frac{M_n}{\rho_{coil} f_{coil} + \rho_{brush} f_{brush}}\right)\frac{1}{N_{av} v_{ref}} \quad (2)$$

where M_n is the total number-average molecular weight of the polymer, ρ_{coil} and ρ_{brush} are the respective mass densities of the coil and brush blocks (see Table 1), N_{av} is Avogadro's number, and $v_{ref} = 118$ Å^3 is the reference volume. In these phase diagrams, the choice of ordinate N/T is a proxy for χN, reflecting the conventionally assumed form $\chi(T) = A/T + B$. Thus, these lyotropic phase diagrams are intended to facilitate comparisons to χN versus f morphology diagrams associated with diblock copolymer melts.

All MP_4 assemblies in the C_1-C_{12} ILs exhibit similar phase progressions, which evolve along the sequence HEX → HEX/GYR → HEX/LAM → LAM with a decreasing φ. This finding suggests that there is not a large difference in the solvent selectivity for the coil or brush homopolymer segments, as simply changing the IL alkyl chain length produces the same

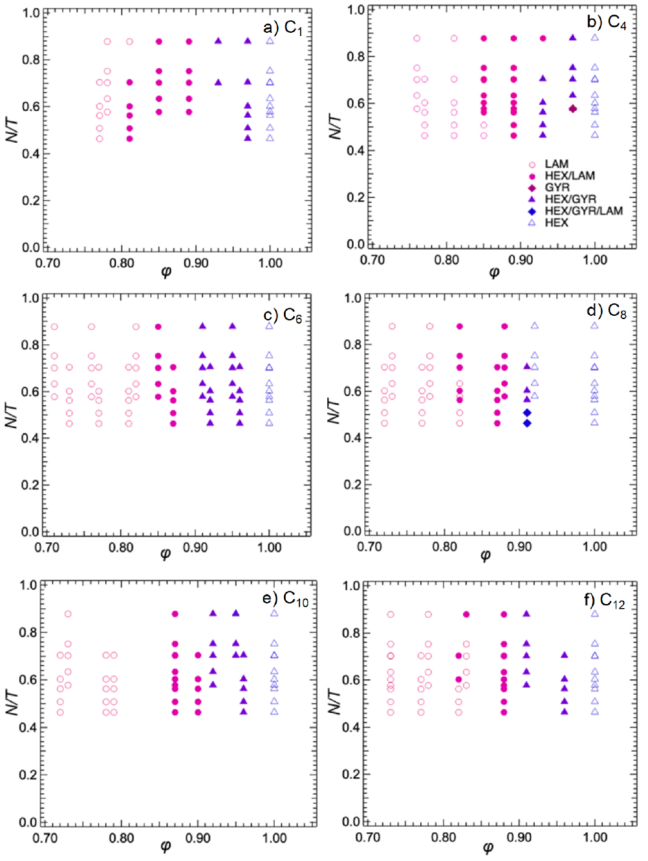

Figure 2. (N/T) *versus* φ phase diagrams of MP_4 in the ILs (a) C_1, (b) C_4, (c) C_6, (d) C_8, (e) C_{10}, and (f) C_{12} exhibiting the general lyotropic phase progression HEX → HEX/GYR → HEX/LAM → LAM with decreasing φ.

sequence of OOTs at nearly the same copolymer volume fractions φ. The HEX morphology notably persists in all samples as a pure phase or as one of the coexisting phases until it gives way to the formation of a pure LAM morphology at the

https://doi.org/10.1021/acs.macromol.3c02451
Macromolecules 2024, 57, 3081−3089

highest IL contents. This finding is somewhat unexpected, given that the Gibbs' phase rule anticipates both pure phase windows and windows of two-phase coexistence in these lyotropic phase diagrams. On that basis, one anticipates windows of pure GYR and GYR/LAM coexistence. However, a pure GYR phase was found in only one as-prepared sample in IL C_4 within the composition resolutions of the reported phase maps.

The predominance of HEX/LAM coexistence suggests that the system is kinetically trapped and favors the formation of coexisting constant mean curvature morphologies rather than NETs that exhibit deviations from a constant mean curvature. This phenomenon may arise from the relatively low nucleation and growth barriers for forming HEX and LAM morphologies, as compared to the larger barrier to forming complex NET phases such as GYR.[58,59] Thus, one might anticipate that HEX/LAM phase coexistence could potentially resolve by changing the sample preparation method or by extended isothermal annealing of the reported samples. Indeed, certain samples do show a change in morphology after annealing at ambient temperature for 15 weeks. For example, Figure 3

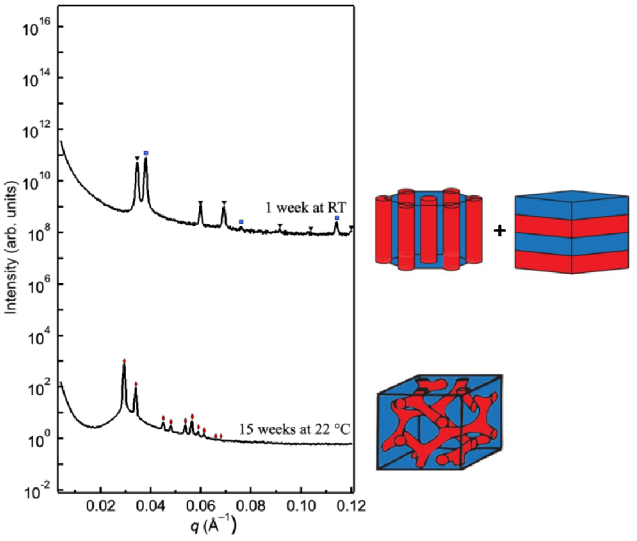

Figure 3. 1D-SAXS patterns of $MP_4(5-10)$ in C_{12} with $\varphi = 0.88$ taken at $T = 180$ °C. Prior to measuring the scattering pattern at $T = 180$ °C, the samples were annealed at room temperature (nominally 22 °C). The top scattering pattern shows the coexistence of LAM (*blue squares*) and HEX (*black triangles*) 1 week after sample preparation, whereas the bottom SAXS pattern was obtained from the same sample after annealing at room temperature for 15 weeks; it became GYR (*red diamonds*).

depicts an SAXS pattern associated with the HEX/GYR coexistence of $MP_4(5-10)$ in C_{12} with $\varphi = 0.88$ after ambient temperature annealing for 1 week. However, extended annealing of this sample on the laboratory benchtop for 15 weeks remarkably results in a phase transformation to a pure GYR phase. We similarly observed that a portion of the samples that initially exhibited HEX/LAM coexistence 1 week after sample preparation transformed into pure HEX phases over the course of 15 weeks, as in Figure S9. Thus, these findings suggests that the thermodynamically preferred phase is not necessarily the one initially observed at "short" time scales, e.g., after isothermal annealing for 24 h at 140 °C and ambient temperature aging for 1 week, if the nucleation and growth barriers for the lowest free energy phase are large.[46] It is worth recalling that one can never "prove" equilibrium in block copolymer samples. For example, in this case, some samples change morphology after three months of annealing, while others do not; there is no obvious correlation with IL volume ratio, IL selectivity, φ, or N/T. All of these variables do affect the self-assembled phase, of course; however, it is not clear that any one of them is responsible for the kinetics of self-assembly. It appears that for a complex morphology such as GYR, there may be an unexpectedly high nucleation barrier, and thus when a GYR morphology is observed, we can assume that the sample has reached a stable state, and it will not subsequently revert to a state of coexistence.

Liberman et al.[56] previously reported a morphology diagram of the coil-brush diblock MP_4, for which they observed the phase sequence HEX → HEX/GYR → GYR → LAM/GYR → HEX/LAM or HEX/GYR/LAM → LAM with increasing coil block volume fraction $f_M = 0.35-0.60$, for samples with no thermally accessible order-to-disorder transition (ODT) that are strongly segregated (high N/T values). On the other hand, more weakly segregated coil-brush diblocks (lower N/T) with accessible ODTs tended to form the expected sequence of composition-dependent pure phases with reduced windows of multiphase coexistence. In the case of PS-*b*-PMMA diblocks loaded with ILs that selectively solvate the PMMA segments, Blakey and coworkers[60] documented substantial increases in the χ_{eff} upon the addition of ILs C_2, C_4, and C_8. Given the structural similarity between PMMA and the M segment in MP_4, which is similarly decorated with a high density of polar methyl ester functionalities, we expect that the IL selectively partitions into the coil domains and thus increases both φ_{eff} and χ_{eff}. Thus, C_x IL incorporation into MP_4 apparently increases the χ_{eff} values substantially, triggering the formation of predominantly coexisting lyotropic mesophases that may or may not be in equilibrium. In the case of kinetically trapped morphologies, the approach to equilibrium could be significantly retarded by the enhanced segregation strength $\chi_{eff}N$ arising from the presence of the IL.

Effect of Solvent Selectivity on the LAM Domain Spacing. The manner in which solvent incorporation affects the self-assembled morphologies of diblock copolymers furnishes information about the solvent selectivity for the two homopolymer segments.[32] Because the morphologies of the neat MP_4 samples are HEX with $f_M \approx 0.38$ and the IL concentration-dependent phase sequence is HEX → GYR → LAM, we deduce that the IL is preferentially incorporated into the M domains and is thus coil-selective. This observation concurs with the reasoning above based on the M chemical structure homology with PMMA, and it is also anticipated by polarity arguments for the components. Hanley et al. previously quantified solvent selectivity by examining how the *d*-spacings of diblock copolymers swollen with block-selective solvents scale with the solvent volume fraction, i.e., $d \sim \varphi^{\alpha}$, where α is an exponent reflecting solvent selectivity.[32,61] They compared their experimentally observed power law dependence for polystyrene-*block*-polyisoprene swollen with tetradecane or various dialkyl phthalates with scaling predictions from self-consistent mean-field theory (SCMFT) for solvents that are increasingly selective for one block and a nonsolvent for the other.[61] They concluded that is maximally $\alpha \approx +1/3$ for LAM in a neutral solvent, whereas the smallest possible $\alpha \approx -1$ corresponds to a completely selective solvent.

https://doi.org/10.1021/acs.macromol.3c02451
Macromolecules 2024, 57, 3081−3089

Therefore, a more selective solvent should exhibit a more negative power law exponent.

This quantitative framework allows us to assess how the IL solvent selectivity in MP_4 changes with C_x *n*-alkyl chain length, using changes in the LAM *d*-spacings of the samples. Accordingly, the *d*-spacing at 22 °C as a function of the IL volume fraction is plotted in Figure 4 for the LAM mesophases

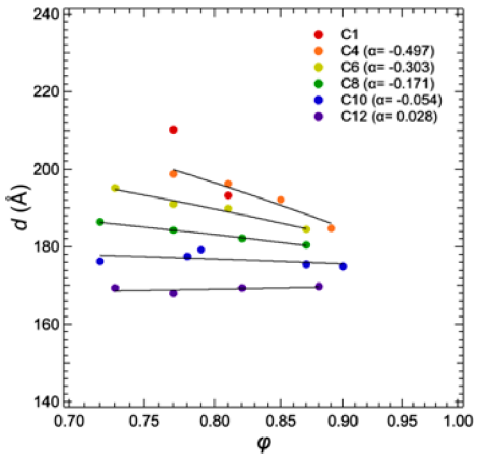

Figure 4. Plot of *d*-spacing vs polymer volume fraction φ at 22 °C, showing how IL solvent selectivity changes with increasing alkyl chain length in LAM morphologies of $MP_4(5-10)$.

of C_x-doped $MP_4(5-10)$ (including samples with LAM coexistence). Here, $d = 2\pi/q^*$ for LAM, where q^* ($Å^{-1}$) is the primary peak position determined by synchrotron SAXS. These analyses show that C_4 exhibits $\alpha = -0.52$, indicating a highly selective solvent, and C_{12} with the longest alkyl chain has $\alpha = 0.03$. Note that the latter result still suggests that the ILs are coil-block selective, as a neutral solvent is expected to have $\alpha = +1/3$.[34] Experimentally, others have reported negative values of α for highly selective IL solvents of diverse structures with various block copolymer chemistries.[46,47,60,62−64] Generally, the values of $-0.52 \leq \alpha \leq 0.03$ recorded here for coil−brush diblocks in C_1-C_{12} ILs are less negative than those documented in earlier studies of linear diblock copolymers with some of the same alkylimidazolium ILs.

Previously studied lyotropic systems involving a selective solvent relied on coil−coil linear diblock copolymers, which exhibit very different chain conformations and extensibilities from the coil−brush systems considered here. Steric considerations along the densely decorated backbone of a bottlebrush generally lead to extended brush backbone chain conformations. The entropy penalty for P_4 brush segment stretching, which scales as the inverse square of its statistical segment length (b), is larger (b_{P4} = 3.3 Å) than for the M segment (b_M = 5.9 Å).[55] Addition of a coil-selective solvent increases χ_{eff}, thus inducing backbone stretching to minimize energetically unfavorable IL/coil contacts with the brush segments. However, the limited extensibility of the majority of the P_4 brush segment constrains the overall increase in the observed LAM *d*-spacing and leads to a lower than expected α value. We speculate that preferential IL localization in the M coil domains induces some small amount of brush chain stretching, thereby flattening the preferred interfacial curvature of the microphase-separated morphology while further stiffening the brush segment. Therefore, the brush-based diblock is less able to accommodate the packing frustration in NETs arising from deviations from a constant mean curvature and consequently the GYR phase window contracts in width at the expense of a wider LAM phase.

The representative plot for $MP_4(5-10)$ in C_8 given in Figure 5 shows a very modest decrease in *d* and a small yet

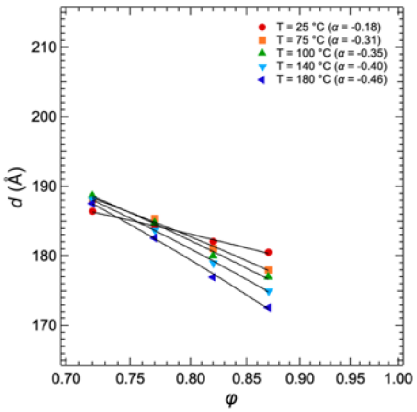

Figure 5. Plot of temperature-dependent *d*-spacings of $MP_4(5-10)$ LAM mesophases as a function of polymer volume fraction φ.

systematic increase in the magnitude of the scaling exponent α with increasing temperature. The former indicates a small reduction in the effective interaction parameter with temperature, possibly implying a predominant effect of entropic contributions to χ_{eff}. On the other hand, the increase in selectivity could imply lower critical solution temperature (LCST) behavior for the brush block in the IL. As these changes in *d* are relatively modest, it is also worth considering the possible role of thermal expansion of each component of the assembly. The coefficient of thermal expansion (CTE) for the C_4 IL is 5.7×10^{-4}/K in the range T = 20−80 °C,[65] whereas the CTE of alkyl substituted and hydrogenated polynorbornenes are $\sim 4 \times 10^{-4}$/K above their T_gs;[66] these two values are of comparable magnitude. Thus, as more IL is added, the average CTE for the sample should increase but only modestly. Using these values to estimate the CTE for each solution, and adjusting the resulting values of *d*, does not change the character of Figure 5, but does slightly reduce the variation in *d* with temperature.

CONCLUSION

Temperature-dependent SAXS studies of the self-assembly behavior of two MP_4 coil−brush diblocks of different molar masses with $f_M \approx 0.38$ in structurally homologous [C_xMIM]-[TFSI] ILs reveal the formation of various lyotropic morphologies, with a relatively weak dependence on the carbon number x of the imidazolium IL *n*-alkyl chain. On initial morphological analyses within 1 week of sample preparation, we observed the phase progression HEX → HEX/GYR → HEX/LAM → LAM regardless of IL identity, except for one instance in >60 samples of a pure GYR phase. Notably, no windows of the GYR/LAM coexistence were noted. This phase sequence, which does not conform to that thermodynamically anticipated by Gibbs' phase rule, suggests that the inclusion of IL into these samples increases their effective segregation strength $\chi_{eff}N$, leading to the formation of kinetically trapped morphologies with remarkably slow structural rearrangement kinetics. Consistent with this, isothermally annealing a HEX/LAM coexistence sample

https://doi.org/10.1021/acs.macromol.3c02451
Macromolecules 2024, 57, 3081−3089

formed in C_{12} for 15 weeks at ambient temperature resulted in a phase transformation to a pure GYR phase.

The relative insensitivity of the boundaries of the observed lyotropic phase windows across the C_x IL series suggests that the solvent selectivity for the coil segment in these architectural asymmetric diblocks only modestly depends on the IL alkyl chain length. By measuring the temperature-dependent variation in the LAM *d*-spacings of these assemblies upon addition of measured amounts of each IL, we found that the solvent selectivity decreases with increasing IL alkyl chain length such that C_4 ($\alpha = -0.52$) is the most selective and C_{12} ($\alpha = +0.03$) is the least selective. The minimal temperature sensitivity of this selectivity over the range $T = 25-180$ °C is consistent with the lack of observed thermally induced order-to-order transitions in the lyotropic samples. Finally, the extent of IL solvent selectivity for the coil block in these coil−brush diblocks is significantly less than that previously reported for lyotropic assemblies of coil−coil diblock polymers. We ascribe these differences to the elastic asymmetry of the architecturally distinct segments of the coil−brush polymers.

■ ASSOCIATED CONTENT

Supporting Information

The Supporting Information is available free of charge at https://pubs.acs.org/doi/10.1021/acs.macromol.3c02451.

Macromonomer and polymer synthesis; characterization of polymers and ionic liquids; additional SAXS patterns of coexisting lyotropic mesophase morphologies and samples after extended annealing; ^{1}H NMR spectra of M monomer in $CDCl_3$, dihydrophytol in $CDCl_3$, *cis*-5-norbornene-2,3-*exo*,*exo*-dicarboxylic acid in $CDCl_3$, P_4 macromonomer in $CDCl_3$, MP_4 coil-brush diblock in $CDCl_3$, SEC-MALS traces for $MP_4(5-10)$; sample ^{1}H NMR spectrum of the ionic liquids used; representative SAXS patterns for $MP_4(5-10)$ in the IL C6 at various temperatures; 1D scattering patterns of $MP_4(5-10)$ and $MP_4(7-13)$; densities used to calculate φ from eq 1; tabulated data from phase diagrams in Figure 2 (PDF)

■ AUTHOR INFORMATION

Corresponding Authors

Mahesh K. Mahanthappa − *Department of Chemical Engineering and Materials Science, University of Minnesota, Minneapolis, Minnesota 55455, United States;* orcid.org/0000-0002-9871-804X; Email: maheshkm@umn.edu

Timothy P. Lodge − *Department of Chemistry, University of Minnesota, Minneapolis, Minnesota 55455, United States; Department of Chemical Engineering and Materials Science, University of Minnesota, Minneapolis, Minnesota 55455, United States;* orcid.org/0000-0001-5916-8834; Email: lodge@umn.edu

Author

Camila Perales Rodriguez − *Department of Chemistry, University of Minnesota, Minneapolis, Minnesota 55455, United States*

Complete contact information is available at: https://pubs.acs.org/10.1021/acs.macromol.3c02451

Notes

The authors declare no competing financial interest.

■ ACKNOWLEDGMENTS

This work was supported by the National Science Foundation through the University of Minnesota MRSEC under award number DMR-2011401. Synchrotron SAXS experiments were performed at the 12-ID-B beamline and the DuPont-Northwestern-Dow Collaborative Access Team (DND-CAT) 5-ID-D beamline of the Advanced Photon Source (APS). DND-CAT is supported by Northwestern University, The Dow Chemical Company, and DuPont de Nemours, Inc. The Advanced Photon Source is a U.S. Department of Energy (DOE) Office of Science User Facility operated for the DOE Office of Science by Argonne National Laboratory under 539 contract no. DE-AC02-06CH11357.

■ REFERENCES

(1) Bates, C. M.; Bates, F. S. 50th Anniversary Perspective: Block Polymers—Pure Potential. *Macromolecules* **2017**, *50*, 3−22.

(2) Bates, F. S.; Hillmyer, M. A.; Lodge, T. P.; Bates, C. M.; Delaney, K. T.; Fredrickson, G. H. Multiblock Polymers: Panacea or Pandora's Box? *Science* **2012**, *336*, 434−440.

(3) Abetz, V. Isoporous Block Copolymer Membranes. *Macromo. Rapid Commun.* **2015**, *36*, 10−22.

(4) Dorin, R. M.; Sai, H.; Wiesner, U. Hierarchically Porous Materials from Block Copolymers. *Chem. Mater.* **2014**, *26*, 339−347.

(5) Bates, C. M.; Maher, M. J.; Janes, D. W.; Ellison, C. J.; Willson, C. G. Block Copolymer Lithography. *Macromolecules* **2014**, *47*, 2−12.

(6) Yang, G. G.; Choi, H. J.; Han, K. H.; Kim, J. H.; Lee, C. W.; Jung, E. I.; Jin, H. M.; Kim, S. O. Block Copolymer Nanopatterning for Nonsemiconductor Device Applications. *ACS Appl. Mater. Interfaces* **2022**, *14*, 12011−12037.

(7) Young, W.-S.; Kuan, W.-F.; Epps, I.; Thomas, H. Block Copolymer Electrolytes for Rechargeable Lithium Batteries. *J. Polym. Sci., Part B: Polym. Phys.* **2014**, *52*, 1−16.

(8) Kim, H.-C.; Park, S.-M.; Hinsberg, W. D. Block Copolymer Based Nanostructures: Materials, Processes, and Applications to Electronics. *Chem. Rev.* **2010**, *110*, 146−177.

(9) Leibler, L. Theory of Microphase Separation in Block Copolymers. *Macromolecules* **1980**, *13*, 1602−1617.

(10) Abetz, V.; Simon, P. F. W. Phase Behaviour and Morphologies of Block Copolymers. *Adv. Polym. Sci.* **2005**, *189*, 125−212.

(11) Matsen, M. W. Effect of Architecture on the Phase Behavior of AB-Type Block Copolymer Melts. *Macromolecules* **2012**, *45*, 2161−2165.

(12) Bates, F. S. Network Phases in Block Copolymer Melts. *MRS Bull.* **2005**, *30*, 525−532.

(13) Meuler, A. J.; Hillmyer, M. A.; Bates, F. S. Ordered Network Mesostructures in Block Polymer Materials. *Macromolecules* **2009**, *42*, 7221−7250.

(14) Thomas, E. L. Nanoscale 3D Ordered Polymer Networks. *Sci. China: Chem.* **2018**, *61*, 25−32.

(15) Schulze, M. W.; McIntosh, L. D.; Hillmyer, M. A.; Lodge, T. P. High-Modulus, High-Conductivity Nanostructured Polymer Electrolyte Membranes via Polymerization-Induced Phase Separation. *Nano Lett.* **2014**, *14*, 122−126.

(16) Li, L.; Schulte, L.; Clausen, L. D.; Hansen, K. M.; Jonsson, G. E.; Ndoni, S. Gyroid Nanoporous Membranes with Tunable Permeability. *ACS Nano* **2011**, *5*, 7754−7766.

(17) Kim, H.; Leal, C. Cuboplexes: Topologically Active siRNA Delivery. *ACS Nano* **2015**, *9*, 10214−10226.

(18) Crossland, E. J.; Kamperman, M.; Nedelcu, M.; Ducati, C.; Wiesner, U.; Smilgies, D. M.; Toombes, G. E.; Hillmyer, M. A.; Ludwigs, S.; Steiner, U.; et al.etal. A Bicontinuous Double Gyroid Hybrid Solar Cell. *Nano Lett.* **2009**, *9* (8), 2807−2812.

(19) Jo, G.; Ahn, H.; Park, M. J. Simple Route for Tuning the Morphology and Conductivity of Polymer Electrolytes: One End Functional Group Is Enough. *ACS Macro Lett.* **2013**, *2*, 990−995.

(20) Werner, J. G.; Rodríguez-Calero, G. G.; Abruña, H. D.; Wiesner, U. Block Copolymer Derived 3-D Interpenetrating Multifunctional Gyroidal Nanohybrids for Electrical Energy Storage. *Energy Environ. Sci.* **2018**, *11*, 1261−1270.
(21) Hajduk, D. A.; Harper, P. E.; Gruner, S. M.; Honeker, C. C.; Kim, G.; Thomas, E. L.; Fetters, L. J. The Gyroid: A New Equilibrium Morphology in Weakly Segregated Diblock Copolymers. *Macromolecules* **1994**, *27*, 4063−4075.
(22) Schulz, M. F.; Bates, F. S.; Almdal, K.; Mortensen, K. Epitaxial Relationship for Hexagonal-to-Cubic Phase Transition in a Book Copolymer Mixture. *Phys. Rev. Lett.* **1994**, *73*, 86−89.
(23) Chu, C.-Y.; Lin, W.-F.; Tsai, J.-C.; Lai, C.-S.; Lo, S.-C.; Chen, H.-L.; Hashimoto, T. Order−Order Transition between Equilibrium Ordered Bicontinuous Nanostructures of Double Diamond and Double Gyroid in Stereoregular Block Copolymer. *Macromolecules* **2012**, *45*, 2471−2477.
(24) Chang, C.-Y.; Manesi, G.-M.; Yang, C.-Y.; Hung, Y.-C.; Yang, K.-C.; Chiu, P.-T.; Avgeropoulos, A.; Ho, R.-M. Mesoscale Networks and Corresponding Transitions from Self-Assembly of Block Copolymers. *Proc. Natl. Acad. Sci. U. S. A.* **2021**, *118*, No. e2022275118.
(25) Chu, C. Y.; Jiang, X.; Jinnai, H.; Pei, R. Y.; Lin, W. F.; Tsai, J. C.; Chen, H. L. Real-Space Evidence of the Equilibrium Ordered Bicontinuous Double Diamond Structure of a Diblock Copolymer. *Soft Matter* **2015**, *11*, 1871−1876.
(26) Takenaka, M.; Wakada, T.; Akasaka, S.; Nishitsuji, S.; Saijo, K.; Shimizu, H.; Kim, M. I.; Hasegawa, H. Orthorhombic *Fddd* Network in Diblock Copolymer Melts. *Macromolecules* **2007**, *40*, 4399−4402.
(27) Tyler, C. A.; Morse, D. C. Orthorhombic *Fddd* Network in Triblock and Diblock Copolymer Melts. *Phys.L Rev. Lett.* **2005**, *94*, 208302.
(28) Matsen, M. W.; Bates, F. S. Origins of Complex Self-Assembly in Block Copolymers. *Macromolecules* **1996**, *29*, 7641−7644.
(29) Reddy, A.; Dimitriyev, M. S.; Grason, G. M. Medial Packing and Elastic Asymmetry Stabilize the Double-Gyroid in Block Copolymers. *Nat. Commun.* **2022**, *13*, 2629.
(30) Alexandridis, P.; Olsson, U.; Lindman, B. Structural Polymorphism of Amphiphilic Copolymers: Six Lyotropic Liquid Crystalline and Two Solution Phases in a Poly(oxybutylene)- *b* -poly(oxyethylene)−Water−Xylene System. *Langmuir* **1997**, *13*, 23−34.
(31) Förster, S.; Berton, B.; Hentze, H. P.; Krämer, E.; Antonietti, M.; Lindner, P. Lyotropic Phase Morphologies of Amphiphilic Block Copolymers. *Macromolecules* **2001**, *34*, 4610−4623.
(32) Lodge, T. P.; Hanley, K. J.; Pudil, B.; Alahapperuma, V. Phase Behavior of Block Copolymers in a Neutral Solvent. *Macromolecules* **2003**, *36*, 816−822.
(33) Yu, G.-E.; Li, H.; Fairclough, J. P. A.; Ryan, A. J.; McKeown, N.; Ali-Adib, Z.; Price, C.; Booth, C. A Study of Lyotropic Mesophases of Concentrated Solutions of a Triblock Copolymer of Ethylene Oxide and 1,2-Butylene Oxide, $E_{16}B_{10}E_{16}$, Using Rheometry, Polarized Light Microscopy, and Small-Angle X-Ray Scattering. *Langmuir* **1998**, *14*, 5782−5789.
(34) Lodge, T. P.; Pudil, B.; Hanley, K. J. The Full Phase Behavior for Block Copolymers in Solvents of Varying Selectivity. *Macromolecules* **2002**, *35*, 4707−4717.
(35) Hanley, K. J.; Lodge, T. P. Effect of Dilution on a Block Copolymer in the Complex Phase Window. *J. Polym. Sci., Part B: Polym. Phys.* **1998**, *36*, 3101−3113.
(36) Ha, S.; La, Y.; Kim, K. T. Polymer Cubosomes: Infinite Cubic Mazes and Possibilities. *Acc. Chem. Res.* **2020**, *53*, 620−631.
(37) Alexandridis, P.; Spontak, R. J. Solvent-Regulated Ordering in Block Copolymers. *Curr. Opin. Colloid Interface Sci.* **1999**, *4*, 130−139.
(38) Li, Z.; Kesselman, E.; Talmon, Y.; Hillmyer, M. A.; Lodge, T. P. Multicompartment Micelles from ABC Miktoarm Stars in Water. *Science* **2004**, *306*, 98−101.
(39) Zhou, C.; Hillmyer, M. A.; Lodge, T. P. Micellization and Micellar Aggregation of Poly(ethylene-*alt*-propylene)-*b*-Poly(ethylene oxide)-*b*-Poly(N-Isopropylacrylamide) Triblock Terpolymers in Water. *Macromolecules* **2011**, *44*, 1635−1641.
(40) Mai, Y.; Eisenberg, A. Self-Assembly of Block Copolymers. *Chem. Soc. Rev.* **2012**, *41*, 5969−5985.
(41) Tamate, R.; Hashimoto, K.; Ueki, T.; Watanabe, M. Block Copolymer Self-Assembly in Ionic Liquids. *Phys. Chem. Chem. Phys.* **2018**, *20*, 25123−25139.
(42) He, Y.; Li, Z.; Simone, P.; Lodge, T. P. Self-Assembly of Block Copolymer Micelles in an Ionic Liquid. *J. Am. Chem. Soc.* **2006**, *128*, 2745−2750.
(43) Simone, P. M.; Lodge, T. P. Lyotropic Phase Behavior of Polybutadiene−Poly(ethylene oxide) Diblock Copolymers in Ionic Liquids. *Macromolecules* **2008**, *41*, 1753−1759.
(44) Early, J. T.; Block, A.; Yager, K. G.; Lodge, T. P. Molecular Weight Dependence of Block Copolymer Micelle Fragmentation Kinetics. *J. Am. Chem. Soc.* **2021**, *143*, 7748−7758.
(45) Brown, R. H.; Duncan, A. J.; Choi, J.-H.; Park, J. K.; Wu, T.; Leo, D. J.; Winey, K. I.; Moore, R. B.; Long, T. E. Effect of Ionic Liquid on Mechanical Properties and Morphology of Zwitterionic Copolymer Membranes. *Macromolecules* **2010**, *43*, 790−796.
(46) Bennett, T. M.; Jack, K. S.; Thurecht, K. J.; Blakey, I. Perturbation of the Experimental Phase Diagram of a Diblock Copolymer by Blending with an Ionic Liquid. *Macromolecules* **2016**, *49*, 205−214.
(47) Chen, X.; Zhou, C.; Chen, S.-J.; Craig, G. S. W.; Rincon-Delgadillo, P.; Dazai, T.; Miyagi, K.; Maehashi, T.; Yamazaki, A.; Gronheid, R.; et al.et al. Ionic Liquids as Additives to Polystyrene-*block*-Poly(methyl methacrylate) Enabling Directed Self-Assembly of Patterns with Sub-10 nm Features. *ACS Appl. Mater. Interfaces* **2018**, *10*, 16747−16759.
(48) Jung, H. Y.; Kim, O.; Park, M. J. Ion Transport in Nanostructured Phosphonated Block Copolymers Containing Ionic Liquids. *Macromol. Rapid Commun.* **2016**, *37*, 1116−1123.
(49) Jung, H. Y.; Park, M. J. Thermodynamics and Phase Behavior of Acid-Tethered Block Copolymers with Ionic Liquids. *Soft Matter* **2017**, *13*, 250−257.
(50) Lodge, T. P. A Unique Platform for Materials Design. *Science* **2008**, *321*, 50−51.
(51) Lodge, T. P.; Ueki, T. Mechanically Tunable, Readily Processable Ion Gels by Self-Assembly of Block Copolymers in Ionic Liquids. *Acc. Chem. Res.* **2016**, *49*, 2107−2114.
(52) Min, J.; Barpuzary, D.; Ham, H.; Kang, G.-C.; Park, M. J. Charged Block Copolymers: From Fundamentals to Electromechanical Applications. *Acc. Chem. Res.* **2021**, *54*, 4024−4035.
(53) Zhang, Y.; Postiglione, W. M.; Xie, R.; Zhang, C.; Zhou, H.; Chaturvedi, V.; Heltemes, K.; Zhou, H.; Feng, T.; Leighton, C.; et al.et al. Wide-Range Continuous Tuning of the Thermal Conductivity of $La_{0.5}Sr_{0.5}CoO_{3-\delta}$ Films via Room-Temperature Ion-Gel Gating. *Nat. Commun.* **2023**, *14*, 2626.
(54) Moon, H. C.; Lodge, T. P.; Frisbie, C. D. Solution Processable, Electrochromic Ion Gels for Sub-1 V, Flexible Displays on Plastic. *Chem. Mater.* **2015**, *27*, 1420−1425.
(55) Liberman, L.; Coughlin, M. L.; Weigand, S.; Bates, F. S.; Lodge, T. P. Phase Behavior of Linear-Bottlebrush Block Polymers. *Macromolecules* **2022**, *55*, 2821−2831.
(56) Liberman, L.; Coughlin, M. L.; Weigand, S.; Edmund, J.; Bates, F. S.; Lodge, T. P. Impact of Side-Chain Length on the Self-Assembly of Linear-Bottlebrush Diblock Copolymers. *Macromolecules* **2022**, *55*, 4947−4955.
(57) Lindsay, A. P.; Mueller, A. J.; Mahanthappa, M. K.; Lodge, T. P.; Bates, F. S. Lodge 1D SAXS Indexing Macro for Igor Pro, 2021. doi.org/10.13020/9m8p-pv93. (accessed 21 November 2023).
(58) Floudas, G.; Ulrich, R.; Wiesner, U.; Chu, B. Nucleation and Growth in Order-to-Order Transitions of a Block Copolymer. *Europhys. Lett.* **2000**, *50*, 182.
(59) Wang, C.-Y.; Lodge, T. P. Kinetics and Mechanisms for the Cylinder-to-Gyroid Transition in a Block Copolymer Solution. *Macromolecules* **2002**, *35*, 6997−7006.

(60) Bennett, T. M.; Chambers, L. C.; Thurecht, K. J.; Jack, K. S.; Blakey, I. Dependence of Block Copolymer Domain Spacing and Morphology on the Cation Structure of Ionic Liquid Additives. *Macromolecules* **2018**, *51*, 8979−8986.
(61) Hanley, K. J.; Lodge, T. P.; Huang, C.-I. Phase Behavior of a Block Copolymer in Solvents of Varying Selectivity. *Macromolecules* **2000**, *33*, 5918−5931.
(62) Simone, P. M.; Lodge, T. P. Phase Behavior and Ionic Conductivity of Concentrated Solutions of Polystyrene-Poly(ethylene oxide) Diblock Copolymers in an Ionic Liquid. *ACS Appl. Mater. Interfaces* **2009**, *1*, 2812−2820.
(63) Hoarfrost, M. L.; Segalman, R. A. Ionic Conductivity of Nanostructured Block Copolymer/Ionic Liquid Membranes. *Macromolecules* **2011**, *44*, 5281−5288.
(64) Virgili, J. M.; Hexemer, A.; Pople, J. A.; Balsara, N. P.; Segalman, R. A. Phase Behavior of Polystyrene-*block*-Poly(2-vinylpyridine) Copolymers in a Selective Ionic Liquid Solvent. *Macromolecules* **2009**, *42*, 4604−4613.
(65) Vranes, M.; Dozic, S.; Djeric, V.; Gadzuric, S. Physicochemical Characterization of 1-Butyl-3-Methylimidazolium and 1-Butyl-1-Methylpyrrolidinium Bis(trifluoromethylsulfonyl)Imide. *J. Chem. Eng. Data* **2012**, *57*, 1072−1077.
(66) Mulhearn, W. D.; Register, R. A. Melt Miscibility in Diblock Copolymers Containing Polyethylene and Substituted Hydrogenated Polynorbornenes. *Macromolecules* **2017**, *50*, 5830−5838.

https://doi.org/10.1021/acs.macromol.3c02451
Macromolecules 2024, 57, 3081−3089